Sensor design and signal processing for an advanced sonar ring

Saeid Fazli and Lindsay Kleeman*

ARC Centre for Perceptive and Intelligent Machines in Complex Environments (PIMCE), Intelligent Robotics Research Centre (IRRC), Monash University, Clayton, VIC 3800 (Australia)

SUMMARY

A conventional sonar ring measures the range to objects based on the first echo and is widely used in indoor mobile robots. In contrast, advanced sonar sensing can produce accurate range and bearing (incidence angle) measurements to multiple targets using multiple receivers and multiple echoes per each receiver at the expense of intensive computation. This paper presents an *advanced sonar ring* that employs a low receiver sample rate to achieve processing of 48 receiver channels at near real time repetition rates of 11.5 Hz. The sonar ring sensing covers 360 degrees around the robot for specular targets for ranges up to six metres, with simultaneously firing of all its 24 transmitters. Digital Signal Processing (DSP) techniques and interference rejection ideas are applied in this sensor to produce a fast and accurate sonar ring. Seven custom designed DSP boards process the receivers sampled at 250 kHz to maximize the speed of processing and to limit memory requirements. This paper presents the new sensor design, the hardware structure, the software architecture, and signal processing of the advanced sonar ring. Repeatability and accuracy of the measurements are tested to characterize the proposed sensor. Due to the low sample rate of 250 kHz, a problem called cycle hopping can occur. The paper presents a solution to cycle hopping and a new transmit coding based on pulse duration to differentiate neighbouring transmitters in the ring. Experimental data show the effectiveness of the designed sensor in indoor environments.

KEYWORDS: Sensor design; Signal processing; Advanced sonar ring; Indoor environments.

I. INTRODUCTION

Sonar ring sensors provide robots with low cost accurate range finders. A sonar ring is a set of sonar sensors configured around the robot to provide sensing of the surrounding environment without the mechanical complication and delays associated with scanning sensors. Conventional sonar rings employ Polaroid ranging modules or equivalent and suffer from poor bearing accuracy and interference problems[1,2]. Furthermore, a fast, accurate and robust environment sensor is always a critical part of robotic tasks such as map building, localization, target tracking and collision avoidance. As an active sensor, sonar has advantages in accuracy, robustness

* Corresponding author. E-mail: (Saeid.fazli | Lindsay.kleeman)@ eng.monash.edu.au

and simplicity when compared with passive methods, such as vision or passive infra red. However, active sensing, and hence sonar, is subject to inter-sensor interference, requiring filtering to prevent erroneous measurements. Research in the past twenty years has progressively refined sonar's accuracy and increased its functionality. Accurate range and bearing measurements of multiple objects have been achieved[3-6], enabling sonar systems to produce accurate maps and to localize the sonar within them. Researchers have developed a sonar ring that allows simultaneous firing and thresholding of echo signals to measure reflectors with a bearing accuracy of around 1 degree[7,8]. Interference can be rejected[4,5,9], making possible the operation of multiple sonars in the same acoustic space, or in noisy spaces. This is important for cooperative robotics, swarm robotics or any time two sonar equipped mobile robots need to pass near each other. Meanwhile, Digital Signal Processor (DSP) systems have enabled the ultrasonic echo to be sampled at 12 bit amplitude resolution and 1 microsecond sample time and then processed in near real time to measure range to 0.2 mm and bearing to 0.1 degrees[10]. This approach is fast and accurate but operates in just one direction within the beamwidth of the transducers. Mechanical scanning and many measurements taken in sequence are needed to cover a full 360 degrees. With the decreasing cost and increasing performance of DSPs, it is now possible to perform intensive sonar echo processing around an entire ring of transducers from a single simultaneous set of transmissions in near real time as presented in this paper. Thus the sequential scanning of the individual sonar sensors has been condensed into one measurement cycle of the advanced sonar ring. The use of DSP local processing relieves communication problems with a host computer as in reference [5] where all echo samples are sent through the computer bus. A second advantage is that the DSP offers optimised instructions for high-speed signal processing over a general purpose computer – in particular the matched filter operations described in this paper are extremely fast. Thirdly, there is little signal degradation since the physical distance between receiver and pre-amplifiers is reduced, allowing much better shielding to the front end of the receiver electronics.

This paper presents the first self-contained sonar ring that achieves accurate and robust distance and range measurements around the robot at near real time rates – termed an advanced sonar ring. Each receiver of advanced sonar ring localizes multiple targets on one firing. This paper describes the hardware design, the software architecture and signal processing of the advanced sonar ring.
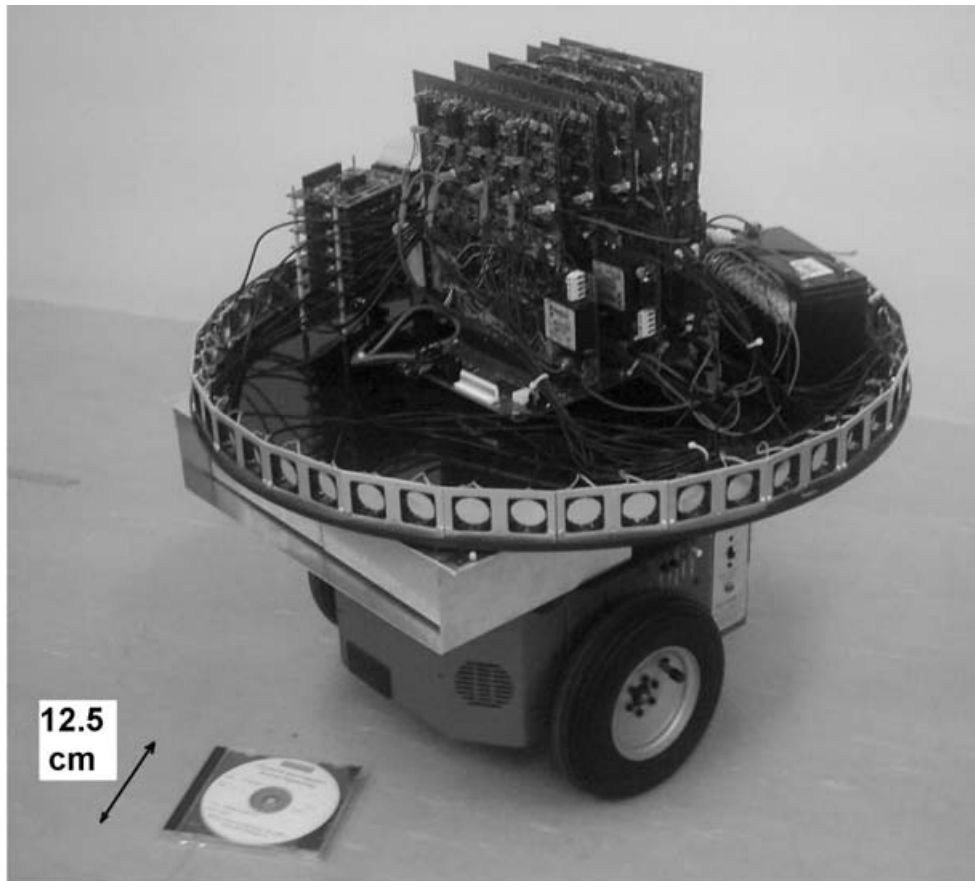
Fig. 1. Advanced Sonar Ring Mounted on an ActivMedia Pioneer 3 DX Mobile Robot.

The repetition rate of the sonar ring is limited by the time of flight to the furthest range of about 6 metres combined in parallel with DSP computation and serial communication between DSPs and a host computer. We achieve a repetition of approximately 11.5 Hz in this paper. Some experimental results and basic sensor description appear in references [11] & [12]. This paper elaborates on the theoretical aspects of the sensor and provides more detailed echo processing and more experimental results than in references [11] & [12]. This paper presents new repeatability and accuracy tests to characterize the sensor.

The custom designed multi DSP sonar ring sensor is shown in Fig. 1 mounted on an ActivMedia Pioneer 3 DX mobile robot. The multi DSP sonar ring consists of 48 transducers in 24 pairs each pair has a transceiver and a receiver so the ring has 24 transmitters firing simultaneously and 48 receivers. The simultaneous firing of a sonar ring has recently been used by other researchers for obstacle detection[13,14]. In the advanced sonar ring, the bearing calculation is based on the difference between arrival time of echo in two receivers and a triangulation technique. As each pair covers approximately 15 degrees, the sonar ring gets information from almost all of the full 360 degrees around the robot as shown in experimental results for field of view in section V.3.

The paper is organised as follows: The next section contains an overview of the sensor, explains the hardware design and introduces all components of the advanced sonar ring. The signal processing of the advanced sonar ring is presented in section III. In this section, also the concepts of template reference point offset table and cycle hopping rejection are explained. Section IV introduces the advanced sonar ring software architecture and the implementation of on-the-fly processing using highly optimised assembly code. This section also explains the implementation of matched filtering within a DSP context, yielding very accurate range and bearing estimation. Experimental results are presented in section V to show the effectiveness of the proposed system. Repeatability and accuracy tests are taken to characterize the sensor. In this section also an idea of interference rejection and the results are described. Conclusions and a discussion of further work are presented in the last section.

II. OVERVIEW OF THE ADVANCED SONAR RING

The advanced sonar ring works by simultaneously firing of all transmitters and hence emitting a burst of ultrasound in all directions, and waiting for the echoes reflected from any objects within the sound beam. Then potential echo sample intervals are extracted from all 48 receivers using a thresholding method. These echo sample intervals are later processed to obtain echo arrival times. To maximize the speed of the sensor and to be able to perform the task in the limited memory of the DSP memory, an interrupt service routine performs thresholding while receivers are listening to echoes. The delays, known as the time-of-flight (TOF), are estimated for all the echoes reflected from different objects to every receiver in each firing. Then the calculated Distance-of-flight (DOF) of the returned echoes is twice the distance

to the object. The bearing angle is determined by combining multiple measurements on different receivers. The basic idea is to calculate TOF for each receiver by means of signal processing technique similar to that used in RADAR[15]. This technique is matched filtering (also called template matching) which is the minimum variance arrival time estimator in the presence of additive white Gaussian noise on the echo. A matched filter is based on finding the peak of the cross correlation of the echo with an *a priori* calculated template. This technique has been extensively used in[3,10,16,17]. The problem of overlapping echoes is not addressed in this paper. However, due to a short pulse length of about 64 μsec, this problem is minimized and the sensor can resolve targets which are separated more than 11 mm apart.

Heale & Kleeman researched a real time DSP sonar echo processor which contains two transmitters and two receivers and was able to sample echoes in 1 MHz, achieving a near real time repetition rate[10]. The design of the advanced sonar ring evolved from that research. The field of view of the Polaroid 7000 transducers used in our work is about 15 degrees, therefore 24 pairs of transducers are considered to cover all around the robot and make it able to estimate the bearing using one transceiver and one receiver in every pair. Six DSP boards called slave PCBs are designed to manage all 48 transducers. Each DSP is processing the echoes returned to eight receiver channels. In order to achieve the same data processing throughput and therefore the same repetition rate, a sampling rate of 250 kHz is used (instead of 1 MHz in reference [10] but for 8 receivers compared to 2 receivers in reference [10]). The lower sampling rate maximizes the speed of processing and limits memory requirements but results in lower accuracy.

Finally, a master DSP is designed to communicate with all slave PCBs and to manage them. A master DSP also in turn relays results of all slaves to a host computer over a serial line. One of the advantages of this configuration is that it relieves the computational burden of the host computer allowing computationally intensive applications to take place on a moving platform. Figure 2 shows an overview of the software structure of the advanced sonar ring.

In the first design, the advanced sonar ring contained both analogue slave and digital slave on the same PCB and ISA bus was considered as communication device but due to the high speed of the Internal Direct Memory Access (IDMA) between slave processors and master processor communication errors were encountered. Therefore, the digital part was re-designed on a four layer board and the analogue slave was separated and PC104 type connector was chosen as the communication bus. In addition, we have encountered problems protecting the Analog to Digital Converters (ADC) from being destroyed through power supply transients and electrostatic discharge during construction. Finally, the digital slaves are re-designed using eight 1-channel ADCs instead of two 4-channel ADCs. The Final hardware design is electronically robust and reliable (Fig. 3). The Power supply of the advanced sonar ring contains a 5 V source to supply six digital slaves and a master, a 24 V battery for the analogue slaves and a 12 V battery for DC-DC converters to produce 300 V bias on the transducers. Power consumption of the batteries are measured as 1.5 W
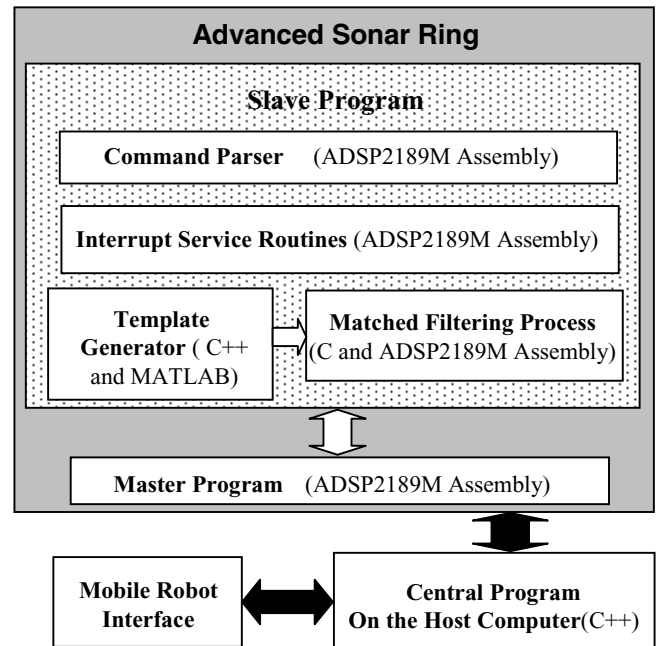

Fig. 2. Overview of the Software Structure.

for the 5 V source, 1.6 W for the 24 V source and 7.7 W for the 12 V source.

The various components of the advanced sonar ring hardware are described below.

II.1. A ring consisting of 48 transducers
A group of eight Polaroid 7000 series transducers, arranged in four pairs, is controlled by a digital slave DSP board and an associated analogue board. The ring contains 24 pairs with each pair containing a transceiver and a receiver 40.5 mm and 15 degrees apart (Fig. 3).

II.2. Six analogue slave PCBs
Each slave board is responsible for controlling the transmission and data acquisition process for four pairs of transceiver and receivers, grouped into four pairs. Also the board contains a high voltage DC-DC converter to produce a 300 V bias on the 8 transducers (Figs. 1, 3).

II.3. Six digital slave PCBs
Each of the six digital slave boards contains a DSP and eight ADCs and connects to an analogue slave board via a ribbon cable (Figs. 1, 3). The DSP is responsible for generating the transmit pulses for the four transceivers and processing the echoes collected by the eight transducers. Eight 12-bit ADCs are configured to allow pairwise synchronised sampling of 8 input channels at 250 kHz sample rate. An AD2189M DSP from Analog Devices Inc. was chosen due to the single clock cycle access to on-chip RAM of 192 k bytes, allowing echoes to be extracted, stored and processed within the DSP chip. The speed of the on-chip memory allows the processor to fetch two operands (one from data memory and one from program memory) and an instruction (from program memory) in a single cycle.
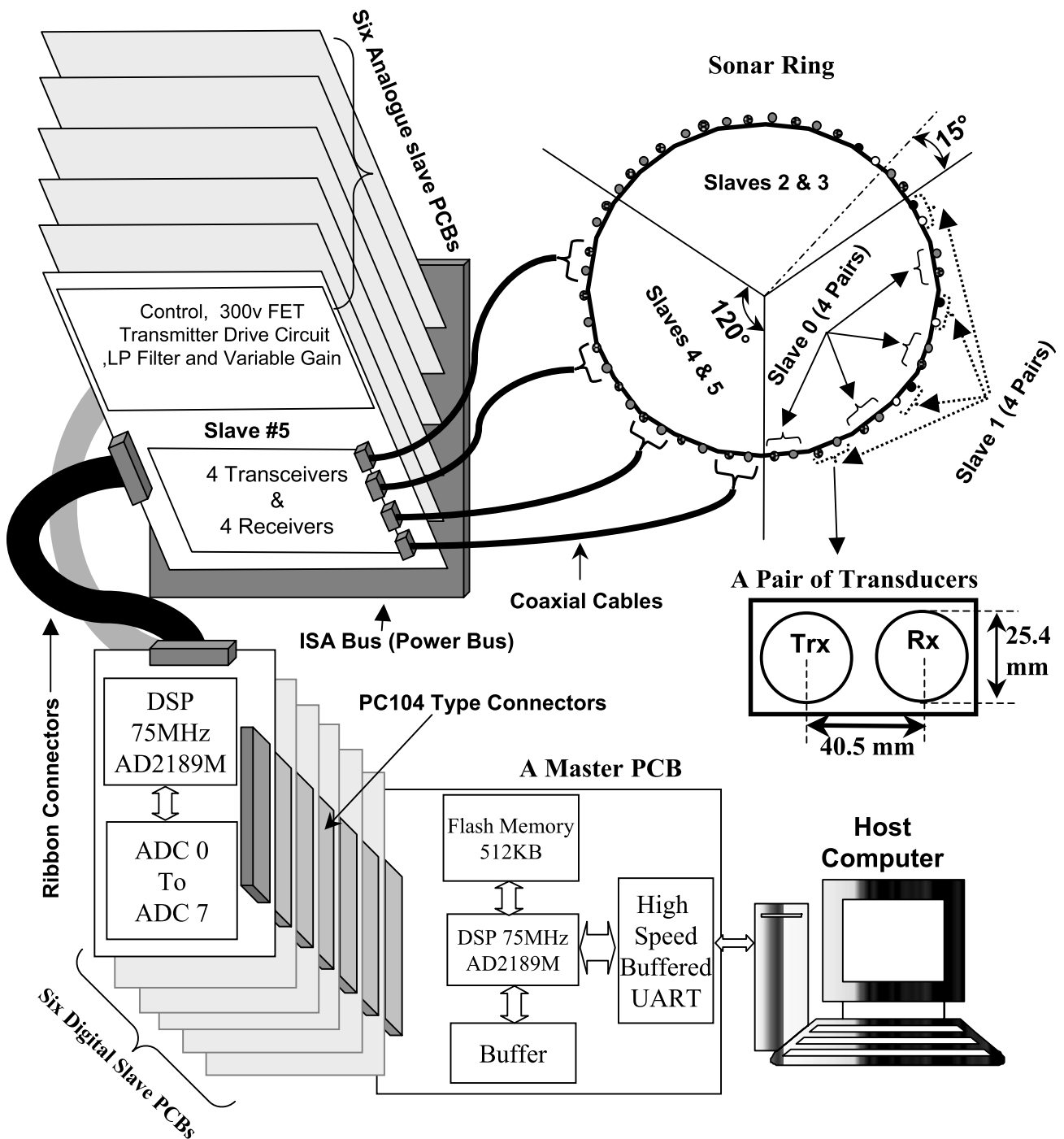
Fig. 3. Overview of the Hardware Structure.

II.4. A master PCB

A master board contains a 2189M DSP from Analog Devices Inc.[18], a flash memory and a high speed buffered UART (Figs. 1, 3). It communicates with a central computer via the high speed serial link and with all the digital slave boards via a PC104 type connector using the IDMA feature of the 2189M DSPs. The DSPs contain two DMA ports, Internal DMA port and Byte DMA port. The IDMA port provides an efficient means of access to the on-chip program memory and data memory of the DSP with only one cycle per word of overhead. The IDMA port has a 16-bit multiplexed address and data bus and supports 24-bit program memory. The

IDMA port is completely asynchronous and can be written to while the ADSP 2189M is operating at full speed[18].

The receiver channels are amplified and low pass filtered before sampling with ADCs at 250 kHz. The transmitter circuitry allows a programmable digital pulse train to be sent to the transducer without the need for preloaded memory buffers as required previously[5]. Instead the slave DSP directly controls the transmit logic every microsecond under interrupt control. Variable gain preamplifiers increase the gain in a fixed profile after each firing to compensate energy lost of the received echo due to ultrasound absorption and dispersion in air[3]. The master board sends all commands and

reads the high level data from slave boards via a PC104 type connector, using IDMA of the DSP which allows high speed access to on-chip memory of the slave DSPs. The master DSP relays results from all slaves to a host computer using a RS232 serial port.

III. SIGNAL PROCESSING FOR THE ADVANCED SONAR RING

The operation of the advanced sonar ring relies solely on TOF information. The TOF is a measure of when received pulse is detected, relative to the time the pulse was transmitted. The performance of this sonar ring in localizing targets depends heavily on the accurate estimation of the TOF. In conventional sonar systems[2,9], a return pulse is detected at a receiver if the received signal exceeds a predetermined threshold. The TOF is the time at which the received signal surpasses the threshold. This method of estimating the TOF is susceptible to noise in the received signal and does not account for the changes in the sonar pulse shape. Consequently, the accuracy of this technique is limited while in reality the accuracy achievable with sonar can be far better[19]. This justifies the use of a more sophisticated method to achieve better accuracy in TOF estimation.

A matched filter is obtained by examining the cross correlation of the echo containing noise with the predicted pulse shape. In this work, we use the approach of Kleeman and Kuc in prediction of the received pulse shapes[3,20]. The arrival time corresponds to the time shifted position of the predicted pulse that gives a maximum in the cross correlation[3,20]. Theory of RADAR shows that the Maximum Likelihood Estimator of the arrival time of the echo corrupted by additive white Gaussian noise is the matched filter[15]. This means that it is usually the best estimator in practice. The problem with the matched filter is predicting the echo pulse shape, since it depends on the bearing angle to the target, dispersion in air of ultrasound, scattering properties of targets and transmitter and receiver characteristics. Linear models exist that accurately predict pulse shape and matched filtering has been implemented successfully[20].

The sonar ring simultaneously fires all 24 transmitters of the ring using a very short square-wave pulse, and analysis simultaneously the waveforms at all 48 receivers using matched filters to accurately determine the arrival time of echoes. The transmitted pulse is 2 cycles of 71.4 kHz plus a counter-timed burst to reduce reverberation in the transducer. The pulse is generated by momentarily removing a 300 V bias, the same as is required to operate the transducers as receivers. A template for one metre range and zero bearing was used as a prototype, and the physical models as in references [3, 21] were applied to generate the templates. Multiple matched filters are required to maintain accuracy because the pulse shape depends greatly on the bearing of the reflector and its range. In fact, this dependence has been utilised for direct bearing measurement[22].

Because pulse shape depends on range and angle of arrival, several filters are generated. Reflections from long range at large angles are unlikely to be detected, and are omitted from the template set. By symmetry, positive and negative angles are indistinguishable. Finally, 13 templates are pre-computed

Table I. Ranges and angles of templates.

Range (m)	Bearing (deg)
1	1, 4, 7, 10
2	1, 4, 8
3	2, 6
4	2, 6
5	2, 6

for varying ranges and angles as shown in table I and saved in the DSPs.

III.1. Offsets in TOF estimation

This section considers discrepancies that arise when TOF is estimated with different angle and range templates. When an arrival echo is nearly equally between two templates in shape, noise in the signal can determine which template better matches an echo. Ideally the same TOF should result from using either different template, however this is not the case in practice as described in this section.

This error is a signal processing artifact due to varying sizes and asymmetric pulse shapes of templates used in matched filtering. In other words, the TOF depends on which template is used in matched filtering. The difference of TOF estimated by a template compared to the reference template (at 1 metre range and 1 degree angle) is defined as an offset in this section.

To find the offset consider the TOF of a template found from correlation with the reference template:

$$ref(t) \otimes template(t) \tag{1}$$

where $ref(t)$ is the reference template, $template(t)$ is another template and the operator $\otimes$ is used for cross correlation. From references [3, 21] the expression (1) can be rewritten as

$$ref(t) \otimes (ref(t)^* h_\theta(t)^* h_\theta(t)^* h_{air}(t)) \tag{2}$$

where h_{air} is the impulse response of sound in air and h_θ is the impulse response of the transducer at an angle of θ to the normal of the transducer.

It can be proved that

$$f(t) \otimes (g(t)^* h(t)) = (f(t) \otimes g(t))^* h(t) \tag{3}$$

Using equation (3), the equation (2) can be rewritten as

$$(ref(t) \otimes ref(t))^* h_\theta(t)^* h_\theta(t)^* h_{air}(t) \tag{4}$$

where the term

$$ref(t) \otimes ref(t) \tag{5}$$

is the auto correlation of the reference template, and can be shown to be an even function, maximized at the origin, therefore

$$\int_{-\infty}^{+\infty} ref(t)ref(t+\tau)\,d\tau \;<=\; \int_{-\infty}^{+\infty} ref^2(\tau)\,d\tau \tag{6}$$
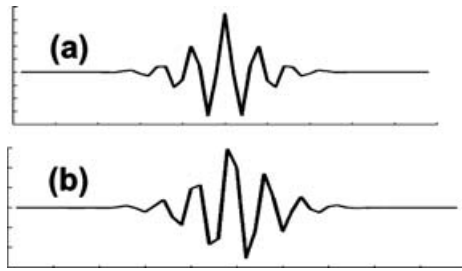
Fig. 4. Cross Correlation of the Reference Template with Another One Meter Template that Results in Symmetry (a) and a Two Meter Template that Results in no Symmetry (b).

the other term

$$h_\theta(t)^* h_\theta(t) \tag{7}$$

is an auto convolution of an even function[3,21] which is the same as an auto correlation and results in another even function, maximized at the origin. Therefore, theoretically, for one metre templates, the maximum correlation occurs at the origin regardless of angle value. For templates with non-trivial term $h_{air}(t)$ (i.e. range > 1 metre), that is not an even function, the maximum correlation may occur at a point shifted from the origin. Figure 4(a) shows the result of cross correlation between the reference template with another one meter range template which results in an even function and 4(b) with a two meter range template which does not result in an even function. In the advanced sonar ring, because we truncate all the templates from both sides after convolution with h_θ, the TOF values are template dependent even for one meter templates. This truncation is necessary to minimize the sizes of the templates and to save DSP memory, and secondly to increase the speed of the template matching process.

In the advanced sonar ring, to solve this offset problem and avoid jumping TOFs, the template for one metre range and one degree bearing is selected as reference template and the start point of that is considered as the reference point of echoes.

The software uses a lookup table called offset table that contains offset values between the reference template and all others. To calculate the offset value, correlation between each template and the reference template is calculated and when maximum correlation occurs, the difference between two start points is calculated and considered as the offset value of that template (Fig. 5). To get sub-sample resolution the above mentioned interpolation method is also used in offset values computation. The offset table is pre-computed and saved with templates. Using offset values the TOF can be written as

$$TOF = 4\,\mu sec(pulse\_peak\_no - template\_peak\_no$$
$$- shift - offset) \tag{8}$$

where *pulse_peak_no* is sample number of the pulse peak and *template_peak_no* is the sample number of the template peak, and in the calculation of the *shift*, sub sample resolution is

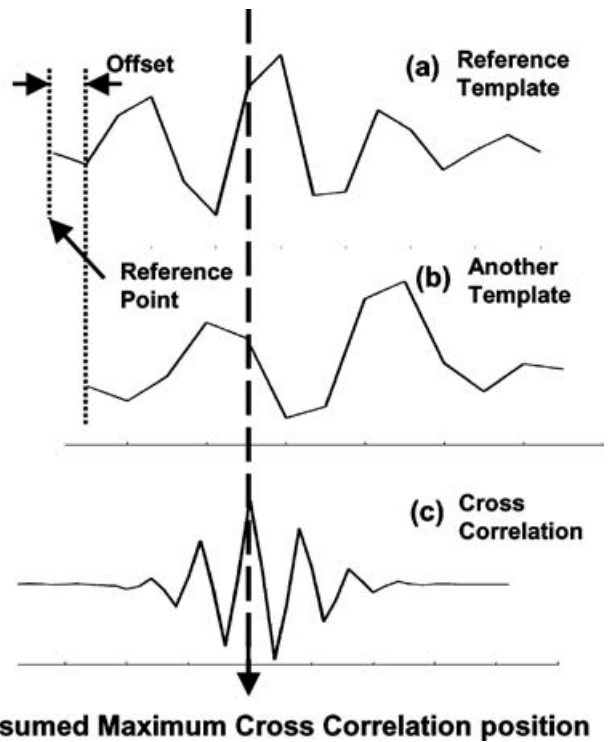

Assumed Maximum Cross Correlation position

Fig. 5. The Definition of the Offset and its Calculation Method.

considered:

$$shift = peak\_dif - \left(\frac{y_2 - 4y_1 + 3y_0}{2(y_2 - 2y_1 + y_0)} - 1 \right) \tag{9}$$

where *peak_dif* is difference between the pulse peak and the template peak in such an alignment that maximum correlation occurs.

When the offsets are not applied, the result of range estimation for a stationary target such as a wall is not consistent and different ranges are calculated when the maximum correlation occurs with different templates. The experimental results, before and after applying this factor are shown in Fig. 6. This problem also occurs when a calculation process of a moving platform or moving target uses different templates due to change in the given range, for example when it uses 1 metre templates and then changes to two meter templates. Therefore the offset table removes the source of these errors.

III.2. Cycle hopping rejection

As explained in previous sections, The matched filtering is performed using 13-samples in the cross correlation between an echo and each of the templates for a given range. If the maximum correlation is greater than 80% then the echo is considered as a reliable echo and the arrival time of the echo is estimated using equation (8). During experiments, we found the position of a stationary object sometimes jumps between two different positions. More investigation of the echoes showed that the maximum value of the cross correlation, which is sampled at the same rate of the echo (4 μsec), occurs in different locations within cross correlation vector, resulting in a varying TOF value caused by a changing shift, described in equation (9). This problem is called cycle hopping
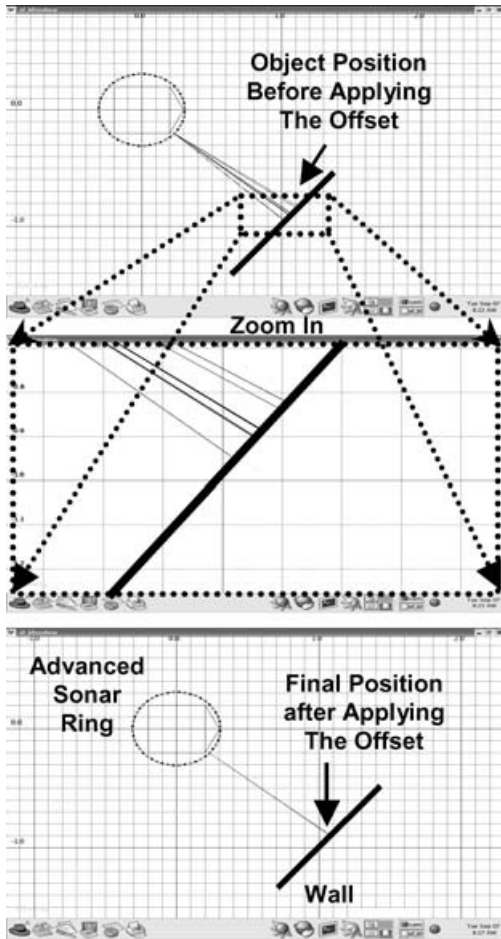
Fig. 6. Experimental Results of Sensing a Wall before and after Applying the Offset Correction.
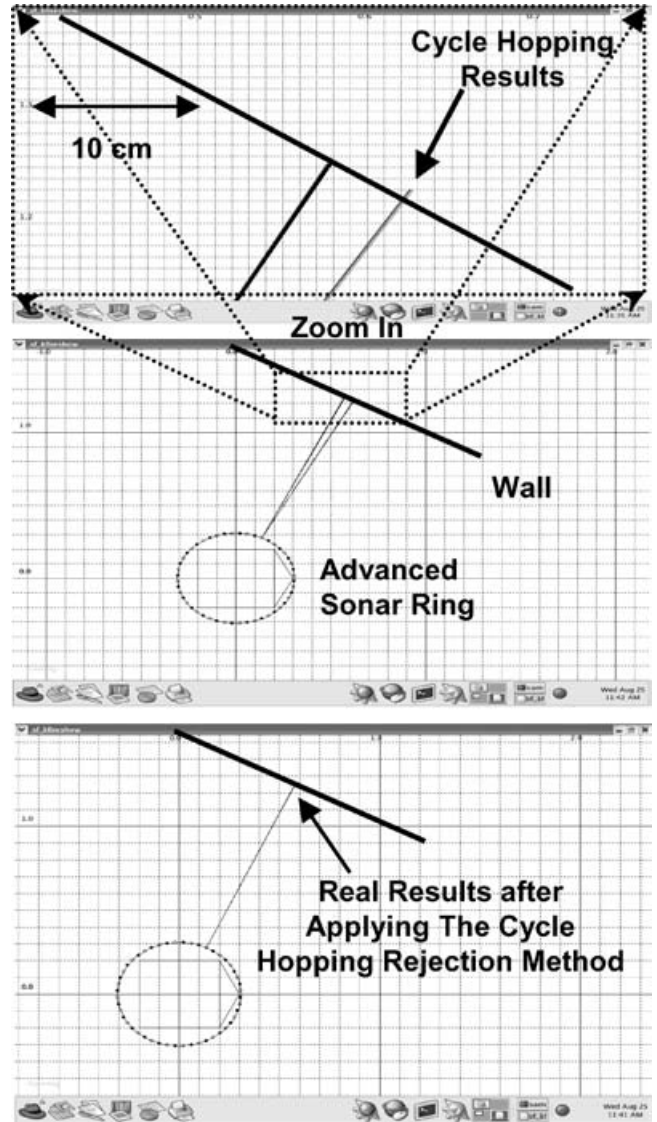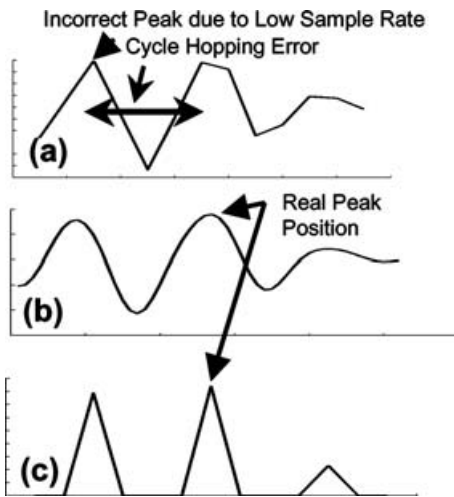

Fig. 7. (a) A Cross Correlation Sampled at 250 kHz and the Cycle Hopping Problem (b) Continuous Time Cross Correlation (c) Real Peak Location using the Interpolation Method on Sampled Data.

Fig. 8. Experimental Data Showing the Effectiveness of The Cycle Hopping Rejection Method.

since the error in shift is usually approximately one wavelength and details are shown in Fig. 7.

The problem arises firstly due to a low sample rate of 250 kHz missing the real peak in the sampling process, and also due to the noise level in the captured echo, which makes the local maxima very close to each other and indistin-

guishable in some conditions. Cycle hopping occurs when the amplitude of an adjacent local maximum is greater than that of the samples calculated around the real peak position.

To solve the problem and to find a genuine peak position within the cross correlation values, an interpolation process is employed after the cross correlation calculation. This process computes a real peak value of the local maxima using a parabolic interpolation over three adjacent samples. Then, the maximum is chosen amongst the results of this process.

Figure 7(a) shows the 4 µsec cross correlation values which has a peak in the wrong position, compared to the other echoes captured from the same target and the same receiver. Figure 7(b) shows the continuous time correlation waveform and the result of the interpolation process on the local maxima is shown in Fig. 7(c). As can be seen, this method can provide a better estimate of the real maximum and avoid the varying TOF.

Experimental results are shown in Fig. 8. This figure shows the effectiveness of the applied method in the real environment. The computed position of each object is
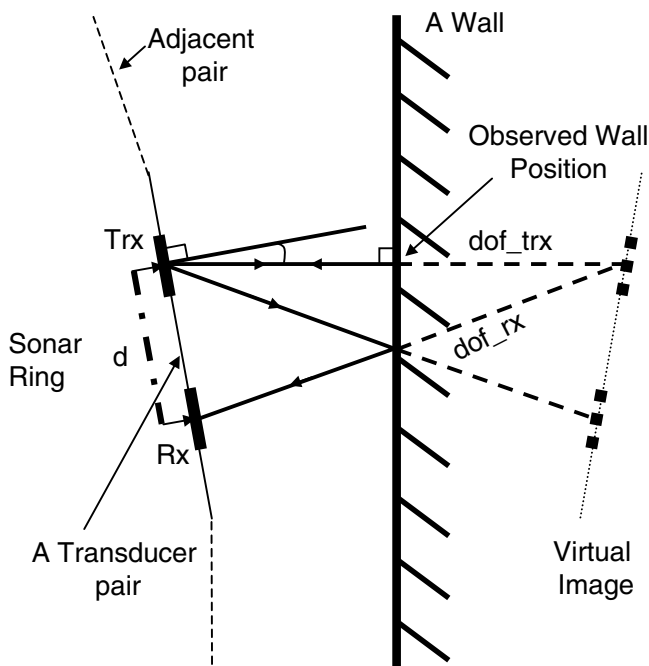
Fig. 9. Virtual Image of a Transducer Pair in a Plane Reflector.

considered at the end of each line. The cycle hopping causes a difference of about 4 samples i.e. 16 microseconds in the arrival time of the echo that corresponds to 2.75 mm difference in the range. As can be seen in Fig. 8, this variation effects the bearing estimation markedly when one of the ranges obtained from a receiver cycle hops.

III.3. Estimating the bearing to targets

The advanced sonar ring includes 24 pairs of transducers, and in each pair one transducer acts as transceiver and another as receiver. To derive the bearing angle to a physical target, a pulse must be received and accepted on both of the receivers of each pair, and correctly associated with each other and the physical reflector. Because the receiver physical spacing is just d = 40.5 mm, the correspondence problem is usually easy to solve, and is simply based on matching the arrival times and pulse amplitudes within predefined ranges.

If both correlation coefficients are over 80% and the ratio of pulse amplitudes is between 0.5 and 2.5 and arrival times differ by less than d* sin(*Max_Angle*)/c = 20 μsec (where *Max_Angle* is taken as 10 degrees) which is consistent with transducers physical spacing, the association is flagged reliable, otherwise it is considered as unreliable and the information may be used for collision avoidance or further process.

Figure 9 shows one transceiver Trx and one receiver Rx of a pair of transducers separated by a distance d which is 40.5 mm in the advanced sonar ring. The distance-of-flights from the reflector to the two transducers are *dof_trx* and *dof_rx*. The bearing angle to the transceiver, θ is determined using the cosine rule.

$$\theta = \frac{\pi}{2} - \cos^{-1}\left(\frac{d^2 + dof\_trx^2 - dof\_rx^2}{2.d.dof\_trx}\right) \quad (10)$$

IV. THE ADVANCED SONAR RING SOFTWARE ARCHITECTURE

The software consists of three parts, a host program, a master program and a slave program. The host program is developed using *C++* under Linux.

The master and slave programs are stored in the flash memory. After turning on the sensor, the master is booted via the byte DMA method of ADSP-2189M. This software is a command parser capable of communication with the host computer and all digital slave boards, allowing the central computer to control all parts of the advanced sonar ring. By sending a command to the master, it can boot all digital slave boards using internal DMA port. A fire command is issued to all slaves simultaneously, thus synchronizing the firing of all transceivers to within a clock cycle of 13 nanoseconds. The software of each slave can communicate with the master by a command parser containing some commands to access low level data. The most important part of this software is an echo processor that is organised into two phases. Figure 10 shows an overview of the DSP processing. During the first stage, assembly code performs on-the-fly processing of the samples from the eight receivers to extract discrete pulses that exceed the noise floor. On-the-fly processing is essential not only to have a real time sensor but also to conserve the on-chip data memory of the DSP. The second stage processes the extracted pulses with C code to extract arrival times using matched filtering.

IV.1. DSP phase one processing – pulse capturing

The phase 1 consists of highly optimised assembly code to extract pulses from eight receiver channels and save them into pulse buffers. This real time program enables approximately 128k words of raw receiver data to be processed in a transmit cycle to yield pulse results within the 48k words of data memory. The software is run while receiving echoes and processes all eight channels within 150 instruction cycles or two microseconds. This phase has a main program and a timer interrupt routine that runs every two microseconds. Each slave board contains eight 1-channel ADCs producing sampled data in 250 kHz. The timer interrupt routine fetches the next 12 bit ADCs samples from the eight receiver channels and places them into eight circular buffers. The interrupt routine is also responsible for generating the transmit pulse.

The main program runs in a loop where each iteration processes the block of data acquired since the previous iteration. The phase 1 processing occurs concurrently with respect to the capture time and consequently must keep up with the incoming data to avoid buffer overflow errors. The eight channels are processed independently through four stages: DC bias removal, thresholding, aggregation and storing into a pulse buffer (Fig. 10).

- Filtering: An optimised high pass software filter removes the DC voltage of echo. This process operates in-place on data in each circular buffer[10].
- Thresholding: An adaptive threshold level is applied to allow for different time varying gains in the receiver preamplifiers resulting in different noise levels. The threshold level is increased when the pulse buffer is fully occupied and is decreased when it is nearly empty. Due
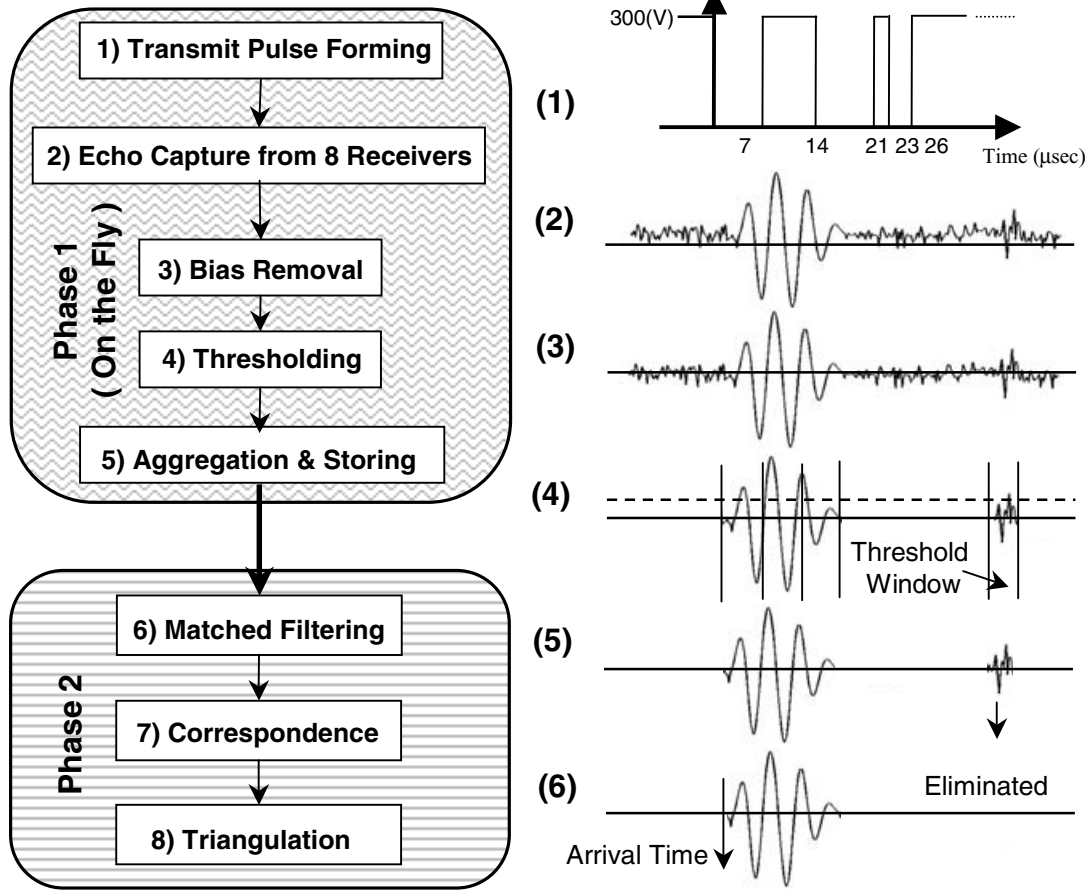
Fig. 10. Overview of Digital Signal Processing.

to limitation in size of each pulse buffer especially in a cluttered environment, this adaptive method is useful from data processing point of view.

- Aggregation and Storing: When there are two or more consecutive blocks exceeding the threshold level, the software merges them along with the resulting ranges (sample numbers) for later template matching. Each receiver channel has its own pulse buffer. Due to the transmitted pulse shape, the length of an echo should be greater than eight samples. If only one block of eight samples is registered as an echo, two blocks which are before and after the block are also considered as part of the echo, then all three blocks are merged and saved into pulse buffer as a potential echo. This helps to keep low energy echoes which are usually reflected from edges or not specular surfaces.

IV.2. DSP phase two processing – matched filtering and bearing estimation

Phase two processing occurs in the DSP after all receiver channels have been logged and stored simultaneously in the pulse buffers. The processing time in this stage occurs in addition to the time of flight between transmitting and receiving the furthest echo – approximately 32 milliseconds. This processing time then directly impacts on the real time performance of the sensor since it takes place sequentially with respect to the capture time (Fig. 10).

To determine the echo pulse arrival times, matched filtering is performed on the echo pulses extracted during phase one of the processing. Template matching obtains the arrival time by cross correlating the received echo pulse with an echo template stored in the DSP. A template is a noise free pulse shape computed offline from a calibration pulse obtained from a plane at one metre range straight ahead. Matched filtering and parabolic interpolation is applied as described in section 3.

After all arrival times are estimated, the bearing estimation is performed for all targets seen by both receivers of each pair using an above mentioned triangulation method. If a target is seen by just one of the receivers it is deemed to be an unreliable target. At the end of the calculation, the slave boards are waiting to be read by the master board and after the high level data of all slave boards are read and sent to the central computer, the master board sends another fire command simultaneously to all the slave boards.

V. EXPERIMENTAL RESULTS

V.1. Repeatability tests

This section presents the performance of the advanced sonar ring in terms of repeatability. Repeatability is the standard deviation of repetitive measurements. The repeatability of range and bearing angle measurements are tested.

Figure 11 shows the standard deviation of range measurements which is obtained by placing an aligned plane at varying distances in front of the sensor. The standard
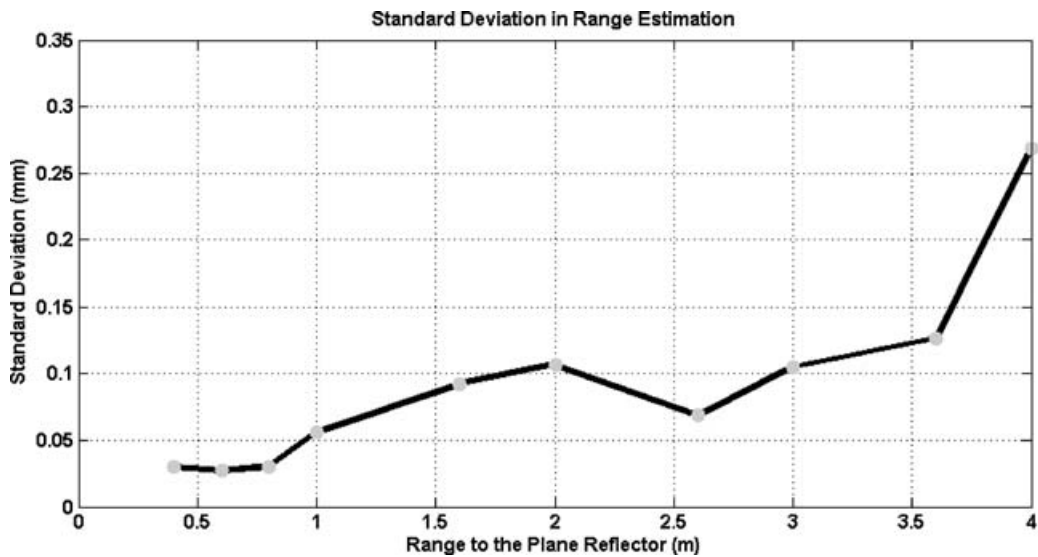
Fig. 11. Repeatability of Range Measurements.

deviation is calculated from a sample of 300 measurements. The graph shows that the standard deviation is less than 0.3 mm for aligned planes that are closer than 4 m.

Figure 12 shows the standard deviation of bearing angle measurements. The results are obtained by placing a plane reflector aligned in front of the sensor at varying distances and measuring it repetitively three hundred times. The standard deviation appears to be less than 0.2 degrees for ranges up to 4 m. The bearing angle to a target is estimated from equation (10).

V.2. *Accuracy tests*

The tests described in this section are designed to calculate the accuracy of the mean measurements of the sensor. We test both the range and bearing accuracies.

a. Test 1 - Range using aligned plane. In this test, a plane reflector aligned in front of a pair of transducers at known

distances from 0.4 m up to 4 m using a calibration jig manufactured for this purpose. Calculated bearing angle was maintained at 0 degrees in order to achieve consistent alignment. At each position 300 samples were recorded. The speed of sound was calibrated by using a straight line fit to the measurements. Figure 13 shows the error in mean range for different positions of the reflector. The error in mean range is less than 0.6 mm for ranges up to 4 m.

This error is mainly attributed to mechanical position error of the plane used in the experiment and variation of the speed of sound during the experiment.

b. Test 2 - Bearing using laser. The accuracy of the bearing angle measurements was measured with the aid of a laser. An optically flat mirror was placed on the centre of the ring to allow it to reflect the laser beam to a measurement screen (Fig. 14). A certain pair of transducers in the ring is used to detect an aligned acrylic plane at range 1 m. The aligned
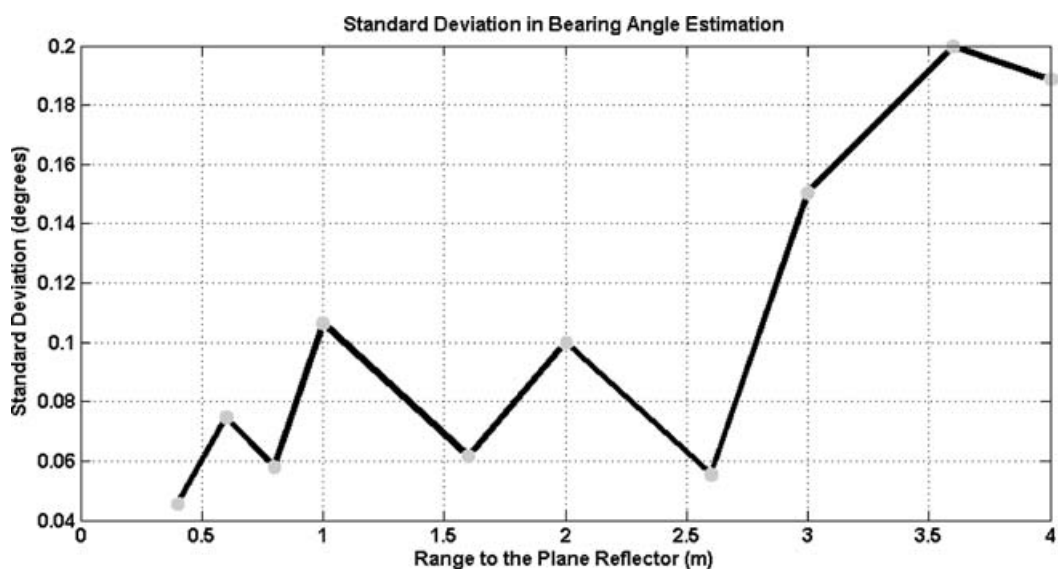

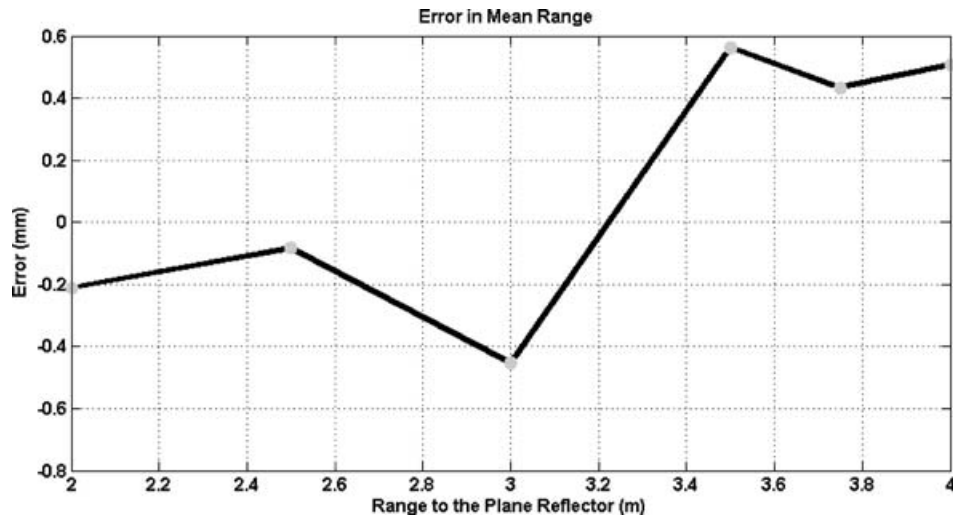Fig. 12. Repeatability of Bearing Measurements.

Fig. 13. Error in Mean Range Estimates.

plane does not obscure the laser since it is below the laser beam and the mirror. Initially, the mirror is positioned parallel to the measurement screen so the laser beam after striking the mirror reflects back on to the laser source. The initial bearing angle to the plane reflector is set to 0 degrees. The measurement screen is adjusted such that it is orthogonal to the initial laser beam path.

Once initially set up, the advanced sonar ring is rotated about the centre of the ring as shown in Fig. 15. To achieve an accurate optical angle estimate from the laser beam, the distance, y, between the sensor and the measurement screen is maximized to 5 m. Now, the sensor detects the plane at a bearing of φ which is equal to the sensor rotation angle. On the other hand, optical measurements estimate that the sensor has been to rotated an angle $0.5 \tan^{-1}(x/y)$. Thus

Fig. 14. Experiment Setup for Testing Accuracy of the Bearing Measurements Using Laser.

we estimate the accuracy of bearing angle measurements by comparing the sensor measured angle φ with the optically measured angle.

Figure 16 shows the error in mean bearing angle at range 1 m. The sensor was rotated from -6 to $+6$ degrees. The error in mean bearing estimation is under 0.17 degrees.

V.3. Field of view
In this section, we present experimental results on the field of view of the advanced sonar ring. The field of view is the region in which the sensor proficiently localises targets. The field of view of the advanced sonar ring depends on the field of view of a pair of transducers. The experimental results are shown in Fig. 17. Within the shaded region, targets are completely detected and localised by the sensor. The figure shows the viewing area for a pair of transducers observing a plane target at positions out to 4 m range. The sensor is capable of covering full 360 degrees around the robot when the effective beamwidth of each pair of transducers is at least 15 degrees and this occurs for highly reflective specular targets at ranges closer than 2.8 m.

V.4. Interference rejection concept and results
In a simultaneously fired sonar ring, multiple transducers must share the same airspace and the pulses transmitted by one transducer may be received by others – this form of interference is also known as crosstalk[14].

When the same sonar pulses are used for all transmitters, a receiver cannot determine whether echoes originate from the same pair or from some other pairs of transducers. The matched filtering of all received pulses possibly results in many phantom objects.

In the advanced sonar ring, each slave board can generate its own pulse shape and therefore using different pulse shapes can potentially eliminate most crosstalk. In this experiment, we divided the transducers into two banks, slaves 0, 2 and 4 as bank 0 and slaves 1, 3 and 5 as bank 1 (see Fig. 3). The two banks are interleaved so adjacent pairs of
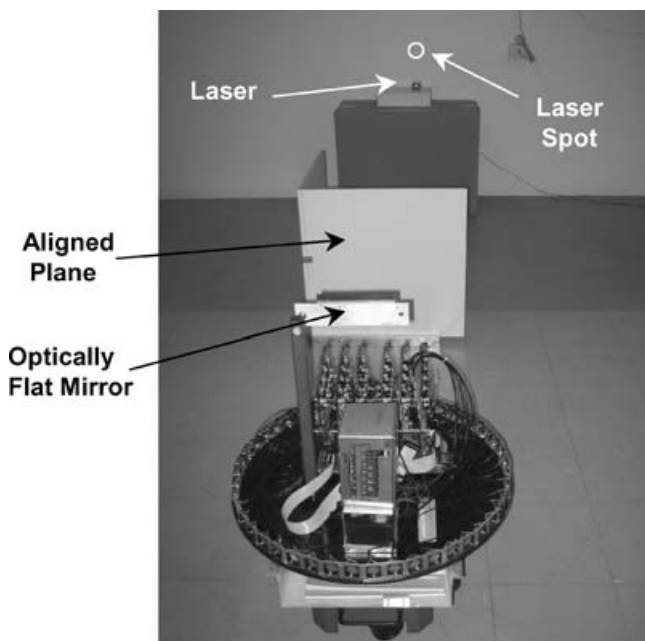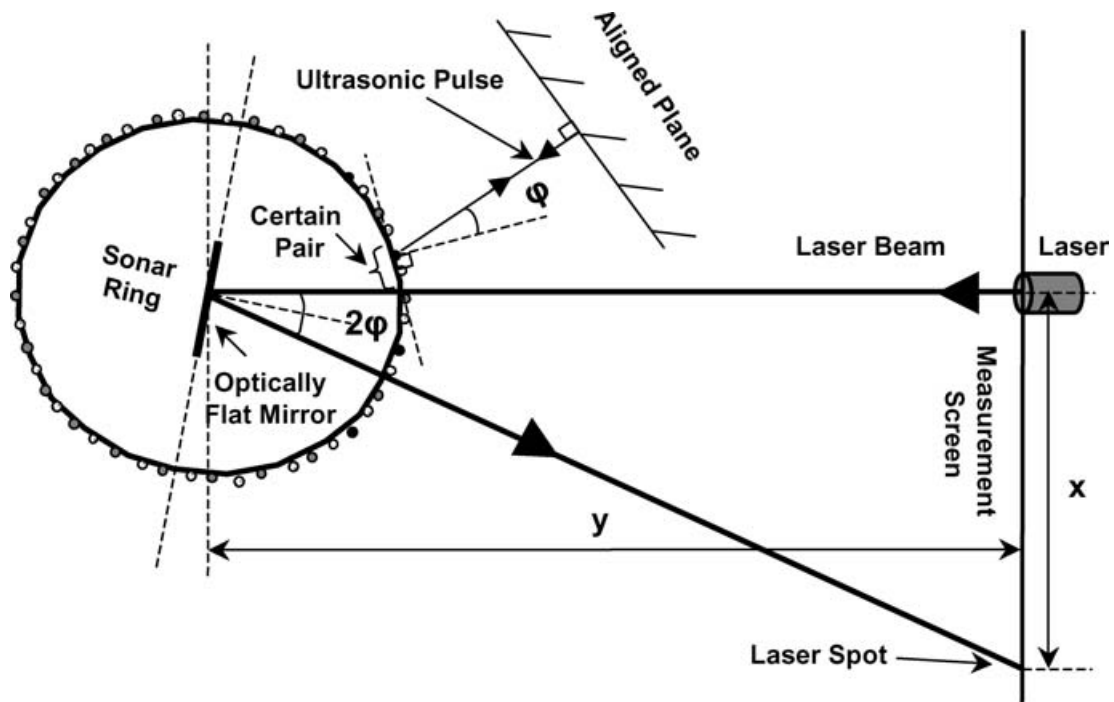
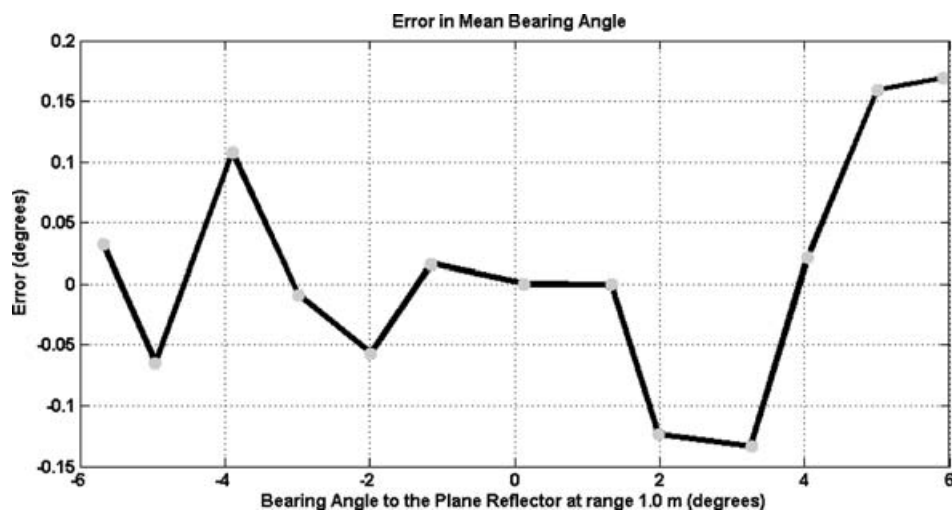Fig. 15. Geometry of Fig. 14 to Measure Bearing Accuracy.

Fig. 16. Error in Mean Bearing Angle Estimates.

transducers belong to different banks. Figure 18 shows voltage waveforms and captured echo pulse shapes of bank 0 and bank 1.

An experimental comparison that shows the advantages of creating different pulse shapes for adjacent transmitters can be seen in Fig. 19. The phantom objects resulting from crosstalk between two banks are eliminated due to significantly lower correlation than genuine echoes (about 60%). In this method, different templates for each bank have been saved in DSP, resulting in rejection of more than 50% of crosstalk. In addition, it is possible to have more banks, i.e. more pulse shapes to achieve better interference rejection but since interference mostly occurs between adjacent pairs, most of the crosstalk is eliminated with just two banks. In fact

multi-path echoes resulted from transmitters of the same bank can not be removed with this method and further processing using a map of the environment is necessary to distinguish them as in reference [17] and also due to wide beamwidth of the pulse no side-lobes occur in the transducer angular beam pattern[3].

VI. CONCLUSIONS AND FUTURE WORK
The paper has presented a new approach to a multi DSP real time sonar-ring sensor based on the real time DSP sonar echo processor[10] and the template matched arrival time estimator that has proven accuracy and robustness characteristics[3]. The performance of the sensor has been illustrated by
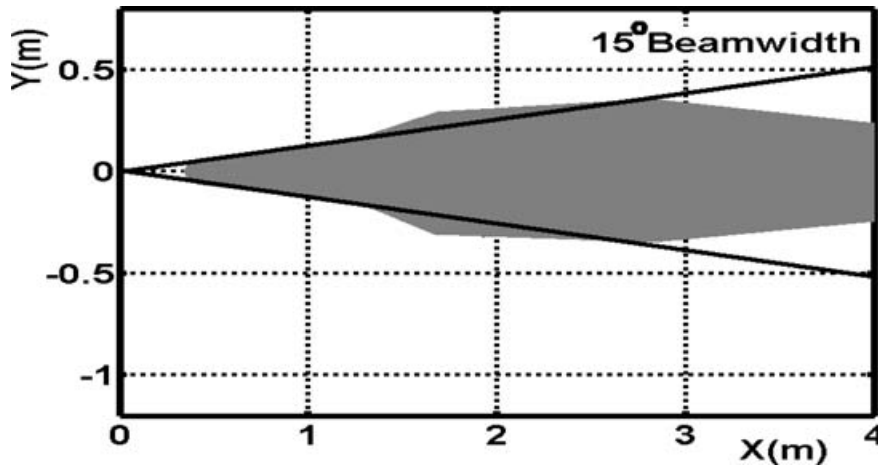
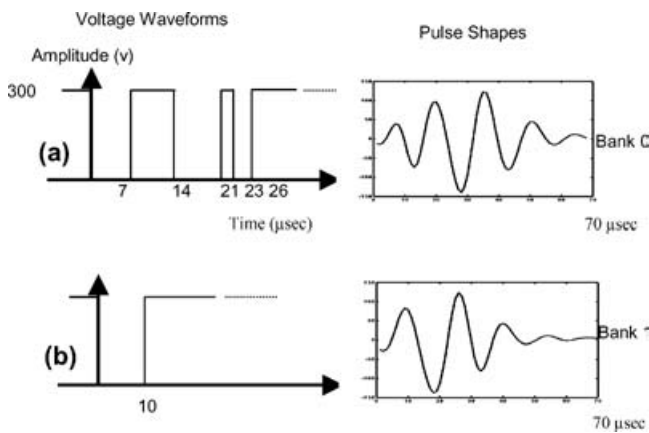Fig. 17. Region of Plane Detectability for a Pair of Transducers.

Fig. 18. Voltage Waveforms Used to drive the Transmitters and Echo Pulse Shapes of Bank 0 and Bank 1 – see Fig. 3.

experimental results. The error in range measurement is less than 0.6 mm and the one of the bearing angle is less than 0.17 degrees.

The new sensor has some advantages. Firstly, processing can be done locally obviating the data communication problem to a central computer. Secondly, due to real time signal processing, central processing can be devoted to higher level applications such as simultaneously localisation and mapping (SLAM). Finally, the sonar ring enables simultaneous sonar sensing of the surroundings of a robot that is useful for on-the-fly applications on moving platforms.

Future work will be concentrated on the implementation of the hardware on FPGA, classification of objects via movement using an extended kalman filter (EKF) and high level applications such as SLAM, obstacle detection and path-planning in real time.
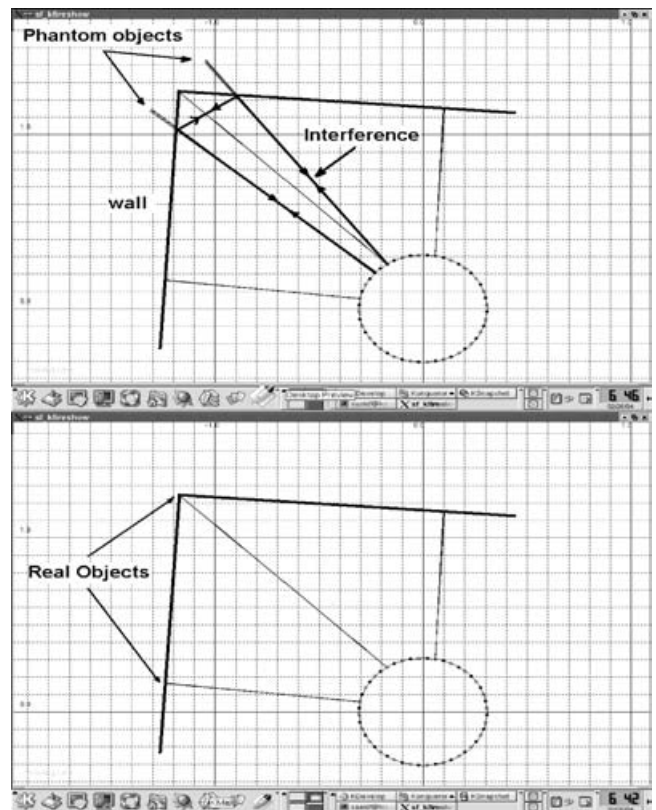
Fig. 19. Target Measurement Results Before and After Applying Interference Rejection.

References
1. J. Budenske and M. Gini,"Why is it so difficult for a robot to pass through a doorway using ultrasonic sensors?" *Proceedings of the 1994 IEEE International Conference on Robotics and Automation*, San Diego, CA, USA (May 8–13, 1994) pp. 3124–3129.
2. T. Tsubouchi,"Nowadays trends in map generation for mobile robots", *Proceedings of the 1996 IEEE/RSJ International Conference on Intelligent Robots and Systems, IROS*. Part 2 (of 3), Osaka, Jpn (Nov. 4–8 1996) pp. 828–833.
3. L. Kleeman and R. Kuc,"Mobile robot sonar for target localization and classification", *International Journal of Robotics Research* **14**, 295–318 (1995).
4. K.-W. Joerg and M. Berg,"Mobile robot sonar sensing with pseudo-random codes", *Proceedings of the 1998 IEEE*

International Conference on Robotics and Automation. Part 4 (of 4), Leuven, Belgium, IEEE (May 16–20, 1998) pp. 2807–2812.

5. L. Kleeman,"Fast and accurate sonar trackers using double pulse coding", *1999 IEEE/RSJ International Conference on Intelligent Robots and Systems (IROS'99)*: *Human and Environment Friendly Robots whith High Intelligence and Emotional Quotients'*, Kyongju, South Korea (Oct. 17–21, 1999) pp. 1185–1190.

6. H. Peremans, K. Audenaert and J. M. Van Campenhout,"High-resolution sensor based on tri-aural perception", *IEEE Transactions on Robotics and Automation* **9**, 36–48 (1993).

7. T. Yata, A. Ohya and S. i. Yuta,"Using one bit wave memory for mobile robots' new sonar-ring sensors", *2000 IEEE International Conference on Systems, Man and Cybernetics*, Nashville, TN, USA (Oct. 8–11, 2000) pp. 3562–3567.

8. T. Yata, A. Ohya, and S. i. Yuta,"Fast and accurate sonar-ring sensor for a mobile robot", *Proceedings – IEEE International Conference on Robotics and Automation*, ICRA99 (May 10–15, 1999) **1**, pp. 630–636.

9. J. Borenstein and Y. Koren,"Error eliminating rapid ultrasonic firing for mobile robot obstacle avoidance", *IEEE Transactions on Robotics and Automation* **11**, 132–138 (1995).

10. A. Heale and L. Kleeman,"A real time DSP sonar echo processor", *2000 IEEE/RSJ International Conference on Intelligent Robots and Systems*, Takamatsu (Oct. 31–Nov. 5, 2000) pp. 1261–1266.

11. S. Fazli and L. Kleeman,"A Real Time Advanced Sonar Ring with Simultaneous Firing", *2004 IEEE/RSJ International Conference on Intelligent Robots and Systems*, Sendai, Japan (Sep. 28–Oct. 2, 2004) pp. 1872–1877.

12. S. Fazli and L. Kleeman,"A Low Sample Rate Real Time Advanced Sonar Ring", *2004 Australasian Conference on Robotics and Automation*, Canberra, Australia (Dec. 6–8, 2004).

13. M. K. Vlastimil MASEK, Aiguo MING and Ljubisa VLACIC,"A New Method to Improve Obstacle Detection Accuracy Using Simultaneous Firing of Sonar Ring Sensors", *The Japan Society for Precision Engineering* **33**, 49–54 (1999).

14. M. K. Vlastimil MASEK, Aiguo MING and Ljubisa VLACIC,"Fast Mobile Robot Obstacle Detection Using Simultaneous Firing of Sonar Ring Sensors", (1998).

15. P. M. Woodward, *Probability and Information Theory with Application to Radar*, 2nd ed. (Oxford: Pergamon Press, 1964).

16. K. S. Chong and L. Kleeman,"Feature-based mapping in real, large scale environments using an ultrasonic array", *International Journal of Robotics Research* **18**, 3–19 (1999).

17. K. S. Chong and L. Kleeman,"Mobile-robot map building from an advanced sonar array and accurate odometry", *International Journal of Robotics Research* **18**, 20–36 (1999).

18. ANALOG-DEVICES, ADSP-2100 FAMILY USER'S MANUAL (Analog Devices, Inc, 1995).

19. H. Akbarally and L. Kleeman,"Sonar sensor for accurate 3D target localisation and classification", *Proceedings of the 1995 IEEE International Conference on Robotics and Automation*. Part 3 (of 3), Nagoya, Jpn (May 21–27, 1995) pp. 3003–3008.

20. L. Kleeman and R. Kuc,"Optimal sonar array for target localization and classification", *Proceedings of the 1994 IEEE International Conference on Robotics and Automation*, San Diego, CA, USA (May 8–13, 1994) pp. 3130–3135.

21. R. Kuc and M. W. Siegel,"Physically based simulation model for acoustic sensor robot navigation", *IEEE PAMI* **9**, 766–778 (1987).

22. T. Yata, L. Kleeman and S. i. Yuta,"Fast-bearing measurement with a single ultrasonic transducer", *International Journal of Robotics Research* **17**, 1202–1213 (1998).